Chemical Engineering Journal 542 (2026) 177624

Contents lists available at ScienceDirect

Chemical Engineering Journal

journal homepage: www.elsevier.com/locate/cej

CO_2 permeation through thermoplastic materials under cryo-compressed conditions for ship-based CO_2 transport

L. Ansaloni [a,1], V. Signorini [b], T.A. Peters [a,*], M. Giacinti Baschetti [b], M. Minelli [b], B. Alcock [a]

[a] SINTEF Industry, Forskningsveien 1, Oslo, Norway
[b] Department of Civil, Chemical, Environmental and Material Engineering (DICAM), Alma Mater Studiorum – University of Bologna, via Terracini 28, Italy

ARTICLE INFO

Keywords:
Thermoplastics
CO_2 permeability
Cryogenic
CO_2 transport
Modelling

ABSTRACT

Transporting CO_2 via ships under cryo-compressed conditions is one of the main scenarios expected for the deployment of the CO_2 transport chain in the coming years. Nevertheless, the performance of non-metallic materials, such polymers that can be used as liners, protective layers, or even as sealing gaskets, under these conditions is scarcely reported in literature, generating knowledge gaps limiting the possibility to take educated decisions during the design of new or the repurposing of existing infrastructure. In this work, CO_2 sorption and permeation behaviour in four thermoplastic polymers (PVDF, PTFE, PEEK, and UHMWPE) were systematically investigated at temperatures down to −46 °C and pressures above saturation. CO_2 solubility in both the gaseous and liquid phases was modelled by means of a thermodynamic framework based on the well-established lattice fluid (LF) and non-equilibrium lattice fluid (NELF) equations of state, enabling the prediction of sorption isotherms beyond the experimental conditions. Despite the different polymer nature, three materials showed an expected behaviour, with permeability dropping at lower temperatures, due to the dominant effect of diffusion over solubility. Nevertheless, a quite peculiar behaviour was observed by PTFE, which displays a transient non-linear trend with local maxima dependent on the operating pressure. Such complex experimental permeability trends observed for the four polymeric materials are accurately described using the Standard Transport Model, aiming to improve the understanding of the experimental results under subcritical and cryo-compressed conditions. The model validation conducted in this study is anticipated to provide a foundation for future modelling efforts, enabling the exploration of system performance beyond current experimental constraints.

1. Introduction

The urgent need to address climate change has brought CO_2 emissions to the forefront of scientific and political agenda. To limit global warming, a rapid transition toward net-zero greenhouse gas emissions is essential, as highlighted by the Intergovernmental Panel on Climate Change [1], since human activities have already caused a temperature rise of approximately 1.17 °C above pre-industrial levels [2]. Among the most effective strategies currently available, Carbon Capture and Storage (CCS) stands out as a key technological pathway to significantly reduce CO_2 emissions from industrial sources while maintaining continuity in essential energy-intensive sectors [3–6]. CCS involves three main steps: capturing CO_2 from industrial emissions, transporting it in a compressed (dense-phase, liquid or supercritical fluid) form, and permanently storing it in suitable geological formations such as depleted oil and gas fields or deep saline aquifers [4,7].

CO_2 transport is a critical challenge as the fluid must be handled in dense or liquid state, meaning under condition of high pressure (up to 20 MPa) or low temperature (down to −50 °C) [8]. Pipelines (preferred for short distances) and ships (more effective in the case of long distances and lower emission capacity, or where pipelines are not feasible) represent the most viable solutions to transfer the captured carbon dioxide between the emission source and the storage site, and the choice of transportation mode depends on the emission capacity and the distance to be covered [8].

Whichever solution is chosen, all metallic and non-metallic components are subjected to extreme operating conditions outside the typical functioning range, leading to a higher risk of leaks and undesired emissions. Moreover, when liquid CO_2 is put in contact with metals (typical choice for pipes, tanks, valves, compressors and pumps), they

* Corresponding author.
E-mail address: thijs.peters@sintef.no (T.A. Peters).
[1] Current address: SLB Capturi, 1360 Fornebu, Norway.

https://doi.org/10.1016/j.cej.2026.177624
Received 8 January 2026; Received in revised form 16 April 2026; Accepted 21 May 2026
Available online 26 May 2026

may be subjected to corrosion problems. This is mainly due to the high acidity of the fluid, especially in the presence of trace amounts of water and other impurities that may not have been completely removed from the compressed stream, thus accelerating the material failure and reducing the service life of the components [9,10].

In this context, engineering thermoplastics are gaining attention for their potential to act as lightweight, corrosion-resistant materials that can serve as barrier layers, liners, seals, or gaskets, to protect infrastructure and prevent gas leakage during the transportation stage [8–13]. The selection of the most suitable materials for CCS application must take into account the polymeric performance for CO_2 transport (low gas uptake and good barrier properties) together with their mechanical resistance and their chemical compatibility, when exposed to such a harsh environment.

Polymer behaviour in contact with highly dense CO_2 varies significantly based on their intrinsic structure which affects both sorption and transport properties. Key factors, in this concern, include morphology (amorphous or semicrystalline), glass transition temperature (T_g), and molecular characteristics such as free volume and phase distribution [14].

During the transport process at low temperature, CO_2 can be absorbed significantly in polymers, potentially affecting their mechanical performance. High CO_2 uptake can lead to significant swelling and softening of polymers, as CO_2 acts as a solvent, increasing molecular mobility and free volume. This may result in a shift in glass transition temperature, increased CO_2 permeability, dimensional mismatch, and a greater risk of deformation or premature failure under loading [15–18]. Additionally, matrix dilation and increased molecular mobility can extract functional additives (e.g., plasticizers, fillers, antioxidants), resulting in permanent changes to polymer properties, reduced lifetime and chemical resistance, and altered gas barrier performance [19–21].

Therefore, great effort was devoted to analyzing the thermodynamic and transport properties of CO_2-polymer mixtures in cryogenic conditions, especially for sorption and permeation isotherms that show CO_2 transitions from gas or gas-like to liquid or liquid-like behaviour. In fact, while CO_2 solubility decreases with temperature, permeability often presents a complex non-monotonous behaviour, resulting from the combination of the trends of solubility and diffusion coefficients [22,23]. Although numerous studies reported CO_2 sorption and permeation in polymers, only a few of them are focused on very low temperature [24,25], mainly due to laboratory experimental limitations, leaving a critical knowledge gap for the sub-ambient performance of polymers in CCS applications.

To bridge this gap, the combination of experimental cryogenic permeation data together with a robust modelling framework, which integrates thermodynamic and transport approaches to describe polymer-penetrant interactions at various temperature, pressure and compositions, provides an effective solution. Specifically, CO_2 solubility in polymers can be rigorously described by the Lattice Fluid Equation of State by Sanchez and Lacombe [26], which proved to work well for the representation of rubbery or molten phases, or the Non-Equilibrium Lattice Fluid model, able to extend the approach to non-equilibrium glassy phases [27]. This is indeed a common situation, at cryogenic temperatures, where most thermoplastics are below their glass transition temperatures. In parallel, gas transport is modelled using the Standard Transport Model (STM), which couples CO_2 solubility with a concentration-dependent diffusivity, governed by a kinetic mobility coefficient and the thermodynamic factor [22,28,29]. This approach captures the effects of penetrant-induced polymer relaxation and enables accurate prediction of permeability across diverse thermodynamic conditions, including liquid-like phases, as it accounts for the changes in diffusion coefficient with concentration [24]. Notably, the model is capable of capturing both increasing and decreasing trends in permeability, as well as non-monotonic behaviours, as observed in the analysis of penetrant transport in glassy polymers, where high CO_2 pressure can lead to a reduction of the glass transition temperature [24,30].

In this work, the permeation behaviour of CO_2 under cryo-compressed conditions (down to −46 °C) is investigated in four polymers, all potentially suitable to be used for CO_2 transport scenarios [31–33]: polyvinylidene fluoride (PVDF), Polytetrafluoroethylene (PTFE), poly(ether) ether ketone (PEEK) and ultra-high molecular weight polyethylene (UHMWPE). For the first time, by integrating gas permeation experiments at low temperature with physically based modelling, this study provides a critical understanding and rigorous assessment of polymer performance under realistic CO_2 transport scenarios. The results offer new insight into the mechanisms governing gas transport at high pressure and low temperature and support informed material selection, design and optimization for safer and more efficient carbon capture and storage infrastructure.

2. Materials and methods

Four examples of different polymeric sheets have been considered for the study: polyether ether ketone (PEEK), polyvinylidene fluoride (PVDF), polytetrafluoroethylene (PTFE) and ultrahigh molecular weight polyethylene (UHMWPE). Their choice has been dictated by the fact that they cover a wide range of thermoplastic materials that can potentially be used in components in CO_2 transport infrastructure under cryo-compressed conditions. While the materials analyzed in this paper are examples of these polymers, it should be considered that variations of morphology and composition such as molecular weight, crystallinity, processing history, filler content and additive packages are likely to affect the performance of polymers in CO_2 applications. Therefore, the analysis presented in this paper may be considered indicative for these particular materials, but not absolute for all variations of these polymers. All samples are analyzed as received, with no pre-treatment. CO_2 permeability at various temperatures and upstream pressures was determined by means of a constant-pressure permeation apparatus (in a similar fashion to the standard method ASTM D3985–17), already described elsewhere [34], connected to a micro gas chromatograph (μ-GC Agilent 990) equipped with a thermal conductivity detector (TCD) which monitors the gas permeate composition (Fig. 1). Permeation experiments were carried out by progressively decreasing the temperature from 20 °C down to −46 °C, while the upstream pressure was increased stepwise from 0 to 20 bar.

The sample is placed in a circular permeation cell (HP Filter Holder, 47 mm, Millipore) with an effective permeation area of 9.6 cm^2. The permeation cell was submerged in a temperature-controlled Julabo FP50 bath for temperature control, where a dedicated low T oil is used (Thermal HL60). On the feed side, the cell is connected to a feed gas system supplying CO_2 by means of a mass flow controller (MFC, Bronkhorst High-Tech), while a back-pressure controller (BPC, Bronkhorst High-Tech, P—512C) is used to control pressure. On the downstream side, Ar is used as sweep gas at a flow rate of 10–20 NmL/min was applied. The permeated gas composition was quantified using a micro gas chromatograph (μ-GC, Agilent 990), equipped with a MS5A and PPU column, and thermal conductivity detectors (TCD) for concentration analysis. The gas permeation (expressed in Barrer, where $1\ Barrer = 3.35 \bullet 10^{-16}\ \frac{mol \bullet m}{m^2 \bullet s \bullet Pa}$) is calculated from the calibrated Argon sweep flow rate and the CO_2 concentration measured by the GC. As an additional control measure, the total permeate flow measured by a mass flow meter (MFM) was used. The permeability coefficient for a given gas (P_i) is calculated as:

$$\mathscr{P}_i = \frac{\dot{n}_p\, y_{i,p}\, l}{A\, \Delta f_i} = \frac{\dot{n}_p\, y_{i,p}\, l}{A\, \left(f_{f,i} - f_{p,i}\right)} \tag{1}$$

where $\dot{n}_p$ is the total molar gas flow on the permeate side calculated from the GC measurement, $y_{i,p}$ is the i-th gas concentration in the permeate side, A is the sample area, l is the sample thickness, and Δf_i is the CO_2 fugacity difference between the feed ($f_{f,i}$) and the permeate side ($f_{p,i}$),

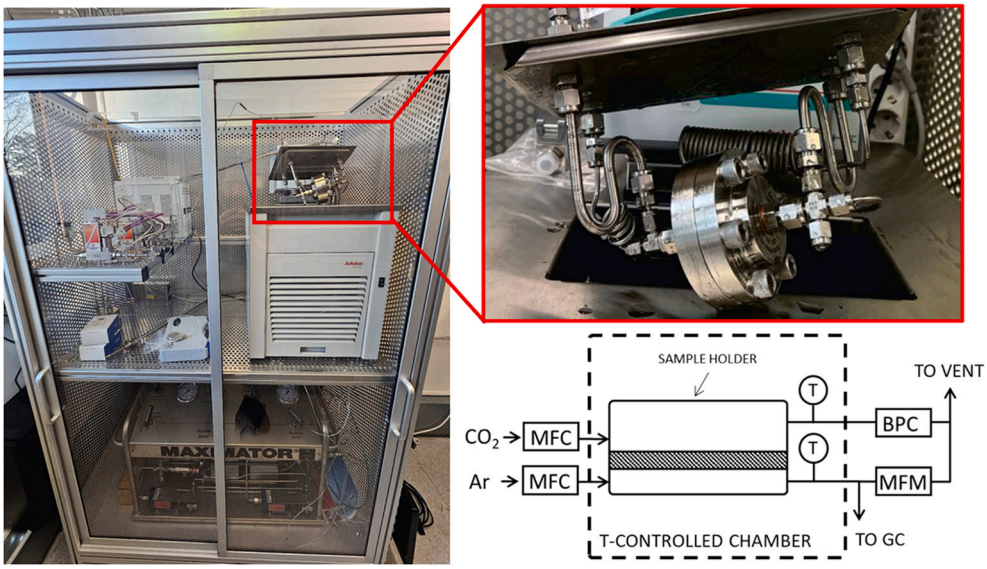

Fig. 1. Setup for cryo-compressed gas permeation in the SINTEF laboratory.

which is at atmospheric pressure (almost negligible with respect to the high upstream pressure at which the test has been conducted). The latter quantity represents the true driving force of the process and it is calculated through the Peng-Robinson EoS for the pure CO_2 phase [35].

The permeation of small molecules through dense polymeric membranes is conventionally interpreted using the solution–diffusion model [36]. In this framework, the overall permeability is defined as expressed in Eq. (2), as the product of a thermodynamic parameter, the solubility coefficient (S), and a kinetic parameter, the diffusion coefficient (D), which are two characteristic parameters of the polymeric material and depend on temperature and pressure.

$$P = < S > \ < D > \tag{2}$$

where the $< >$ sign indicates that such properties must be properly averaged on the membrane thickness. Solubility and diffusion coefficients can be determined experimentally by exploiting the pressure decay technique, which has been used in the present work to complement direct permeation tests [34,37]. A detailed description of the custom-made apparatus and the procedure for transient sorption experiments is provided in the Supporting Information (SI), together with the equations and calculation methods used to determine solubility and diffusivity. Briefly, the experiments were carried out in a stepwise (differential) manner by progressively increasing the pressure from 0 to 30 bar, while the temperature was varied from 5 to 45 °C. The analysis is based on a manometric technique, in which a pre-weighed polymer sample is placed in a dead-end chamber and gas sorption is quantified from the pressure decay in the closed, calibrated volume as the penetrant dissolves into the polymer matrix. Moreover, the time evolution of pressure was used to evaluate sorption kinetics and to determine the diffusion coefficient (D) in the dense polymer layer, modelled as a planar sheet using the analytical solution of Fick's law [38]. The experimental uncertainty associated to those measurements can be estimated approximately 5% for gas solubility, while a larger error (about 10%) can be attributed to the diffusivity values. Error values reflect both the intrinsic variability of the measurements and the limitations related to the experimental dataset.

3. Model description

3.1. Gas solubility: thermodynamic equation of state (EoS) approach

The calculation of gas solubility in polymers can be effectively carried out using Equation of State (EoS) models, which relate chemical potential of the penetrant in the gas phase and within the polymer matrix to pressure, volume, temperature, and internal energy of the system or mixture [26,39,40].

In this context, the Lattice Fluid (LF) theory developed by Sanchez and Lacombe [26] provides a robust framework for describing the thermodynamic behaviour of gas–polymer systems in the amorphous or molten state (for semicrystalline polymers, only the amorphous phase is considered permeable, with the crystalline regions assumed to be impermeable to gas molecules [19,41]), although a distinction must be made based on whether the polymer is in a rubbery or glassy state.

In rubbery polymers, i.e. polymers which are above T_g at the application temperature, equilibrium is rapidly established, and so the Sanchez–Lacombe EoS can be used predictively to evaluate the volume of polymer–penetrant mixtures and the associated polymer swelling. Conversely, glassy materials, i.e. polymers which are below T_g at the application temperature, such as PEEK, exist in non-equilibrium states and retain excess free volume [42,43]. To address these conditions, Doghieri and Sarti introduced the Non-Equilibrium Lattice Fluid (NELF) model [27], which extends the LF theory by incorporating polymer density as a further internal state variable (Eq. 4S in SI). In fact, while for polymers above T_g (i.e., rubbers at equilibrium), density can be directly derived from the equation of state, for polymers in the glassy state—non-equilibrium systems by nature—the polymer mass density ρ_{pol} is an input parameter:

$$\rho_{pol} = \rho_{pol}^{eq}\,(T, p, \Omega) \tag{3}$$

The main result of this thermodynamic procedure is that the Helmholtz free energy density, a^{NE}, does not depend on the pressure of the system, but only on composition and polymer mass density [44]. This comprehensive approach allows for the calculation of the free energy of the system under non-equilibrium conditions, thus enabling the accurate modelling of gas sorption in glassy polymers.

As for any equation of state, the CO_2 solubility, has been obtained by the resolution of phase equilibrium between the polymer and the penetrant phases, as expressed by Eq. (4):

$$\mu_i^{pol}\left(T, p, \Omega_i, \rho_{pol}\right) = \mu_i^{gas}\,(T, p) \tag{4}$$

where μ_i^{gas} represents the chemical potential of the penetrant i in the pure gas phase as a function of temperature and pressure, while μ_i^{pol} is that in the polymer phase, which requires also the knowledge of the

composition Ω_i.

As already reported in other studies [30,45–49], for both SL and NELF models, the phase equilibrium between penetrant and polymer quantities is determined using three independent parameters for each component, namely: the characteristic temperature T^*, the characteristic pressure p^* and the close-packed density ρ^*, that may be estimated from standard pressure-volume-temperature (pVT) data.

By applying the mixing rules of the thermodynamic equation of state for the description of polymer/penetrant mixture (Table 1S in the Supporting Information), the binary interaction parameter k_{ij} is identified by a single mixture information, which relates the gas and polymer specific intermolecular interaction [26,50].

Moreover, due to their inherently non-equilibrium state, glassy polymers exhibit densities lower than those predicted at equilibrium, making conventional EoS models inadequate for their thermodynamic description. Equilibrium EoS are indeed unable to describe the swelling induced by sorbed penetrant, which is essential for determining the solubility isotherms. For this reason, an independent relationship is introduced, through the definition of a swelling coefficient (k_{swell}), to describe quantitatively the density pressure relationship in the glassy state (Eq. 5). From experimental findings, density tends to follow a linear trend with respect to the partial pressure of the gas, a single parameter is therefore sufficient to describe its behaviour.

$$\frac{1}{\rho_{pol}(T,p)} = \frac{1 + k_{swell}(T,p)\, p_i}{\rho^0_{pol}\,(T,p)} \tag{5}$$

In which ρ^0_{pol} and k_{swell} represent the "dry" polymer density and the swelling coefficient, respectively, which are functions of temperature and pressure [51,52].

Moreover, in semi-crystalline polymers, as the case of the polymers considered in this work, the larger density of crystals makes these domains practically impermeable to permeating species, meaning that only the amorphous part of the matrix is involved in the gas uptake and transport. Therefore, one has to account for the presence of crystals considering the degree of crystallinity (χ_c) and determining the solubility in the amorphous phase only, which will be used in the thermodynamic analysis:

$$\Omega_{am} = \Omega_{sc} \bullet (1 - \chi_c) \tag{6}$$

where the subscripts *sc* and *am* denote semicrystalline and amorphous phases, respectively.

3.2. Gas permeability: Standard Transport Model (STM) for CO_2 transport

As with sorption isotherms, the permeability of both rubbery and glassy polymers can be effectively predicted using the Standard Transport Model (STM), which offers a robust framework by integrating thermodynamic and kinetic contributions to describe gas transport [22]. Within this approach, the mass flux of a penetrant across a polymer membrane is governed by the product of the chemical potential gradient—serving as the driving force—and the mobility coefficient L, as outlined in Eq. (7).

The mobility coefficient encapsulates the kinetic resistance encountered by the penetrant molecules as they migrate through the polymer matrix. This parameter is influenced by intrinsic properties of both the polymer and the penetrant, as well as by the local concentration of the sorbed species. Consequently, the STM provides a physically meaningful and predictive method for analyzing gas permeation behaviour under various operational conditions, as a function of polymer density ρ and the absorbed mass fraction of the gas Ω_i.

$$J_i = -\rho L \Omega_i \nabla\left(\frac{\mu_i}{RT}\right) \tag{7}$$

The mobility L is affected by the presence of penetrant dissolved in the polymer matrix, and an exponential dependence on gas concentration is proven to be effective, as follows [27]:

$$L = L_\infty e^{\beta\Omega} \tag{8}$$

where L_∞ is the infinite dilution mobility coefficient and β is the plasticization factor, which represents the increase in L inside the polymer upon swelling, as a consequence of the enhanced free volume and mobility of the polymer macromolecules.

Mobility coefficient is clearly related to diffusion coefficient, as defined by Fick's law; the two quantities are correlated by the thermodynamic factor α, which can be readily calculated either from experimental sorption isotherms or from thermodynamic model (Eq. 9) [29]:

$$D = L\frac{\partial \mu_i / RT}{\partial ln \Omega_i} = L\alpha \tag{9}$$

The diffusion of low molecular weight species i in binary (or pseudo-binary) mixtures can be used as a key point for the semi-empirical model description of gas permeability in glassy polymers. In this concern, at steady state condition, where the upstream surface, at $x = 0$, is kept at partial pressure p_i^u and concentration Ω_i^u, and the downstream side ($x = l$) is kept at partial pressure p_i^d and concentration Ω_i^d, the diffusive mass flux is constant throughout the membrane and, by recalling the permeability definition, one can express the permeability by the following model equation, rescaled on the fugacity gradient through the membrane thickness:

$$P_i = \frac{1}{\left(f_i^u - f_i^d\right)} \int_{p_i^d}^{p_i^u} \rho L_\infty e^{\beta\Omega_i} S_i\, z_i\, dp_i \tag{10}$$

where z_i represent the compressibility of the pure gas phase calculated at the different operative temperatures and pressures by means of the Peng-Robinson EoS; while S_i stands for the gas solubility coefficient (where $S_i = \frac{\Omega_i}{p}$), calculated by the EoS (as described in the previous section) [23,28].

The semi-empirical nature of the Standard Transport Model (STM) for permeability enables the integration of sorption and transport data. By solving the phase equilibrium and incorporating thermodynamic modelling, the STM allows for accurate prediction of permeability behaviour in polymeric materials across a broad range of temperatures and pressures [53].

When applying the LF/NELF model or using experimentally derived solubility isotherms, both the thermodynamic factor α and the penetrant fraction Ω_i can be written as a function of the upstream penetrant pressure. Consequently, eq. (10) serves as a predictive tool for calculating permeability when L_∞ and β, are available, for instance, derived from diffusivity data at different temperatures, thus allowing a full prediction of permeability. Alternatively, it can be employed to estimate L_∞ and β, from a limited set of permeability measurements, before extending the modelling analysis to describe the behaviour of permeability isotherms over a broader range of conditions.

An estimation of the uncertainty associated both to the LF/NELF solubility isotherms and STM model is performed using the symmetric mean absolute percentage error (sMAPE),as in Eq. (11):

$$sMAPE = \frac{1}{n}\sum_{i=1}^{n}\frac{|y_i - \hat{y}_i|}{|y_i| + |\hat{y}_i|} \bullet 100 \tag{11}$$

where $\hat{y}_i$ is the predictive value obtained through the model (either LF/NELF or STM), y_i is the experimental data and n is the number of data points. The sMAPE values for all parameters are presented in Table S2. Overall, our analysis suggests that these values remain under 10% and only marginally exceed this limit in rare cases, supporting the model's accuracy.

4. Results

4.1. Materials

The main characteristics of the four thermoplastic materials studied in this work are reported in Table 1. Properties for PTFE and PVDF are taken from previous work [34], while that of PEEK are measured by using a TA Instruments DSC2500, using the same method already reported [34].

4.2. Low temperature permeability

Table 2 summarizes all the characteristic parameters required for the application of LF/NELF equations. The modelling analysis relied on the characteristic parameters T^*, p^* and ρ^* of the equilibrium Sanchez-Lacombe theory for the pure components, both for the polymers and CO_2. The gas parameters are often fitted to saturated vapour pressure and liquid density VLE data [55], while those of the polymers are usually obtained from the best-fit of pressure–volume–temperature (pVT) data in the equilibrium conditions (Fig. 3S in SI), i.e. above the glass transition temperature (T_g) and in the pure amorphous state (above the melting point). In the present work, the values are either retrieved from literature [24,34,41,56] or evaluated from pVT data by Zoller [56] as reported in Table 2. In this concern, it should be noted that the characteristic parameters used for UHMWPE were taken equal to that of high-density polyethylene (HDPE), since they shared the same structure, in the lack of direct experimental pVT data available [41].

Fig. 2 reports the experimental permeability data, calculated using the CO_2 fugacity difference as driving force (Eq. (1)), at steady state obtained for (a) PVDF, (b) PEEK, (c) PTFE and (d) UHMWPE as a function of temperature and upstream pressure. From the comparison of the four materials considered, PTFE shows the highest permeability, with values higher than 20 Barrer at 20 bar and temperatures between −18 to −30 °C, while PVDF and PEEK exhibit lower permeability in the range between 0.01 and 1 Barrer at all temperatures. Importantly, after exposure to liquid CO_2 at low temperatures, the materials do not show significant changes in transport performance. This was verified by conducting a second permeability measurement cycle under identical conditions (Fig. 2S in the Supporting Information). The results indicate that, for most materials, the permeability, diffusion and solubility coefficients remain comparable to those obtained in the first experimental run. The maximum relative standard deviation associated with repeatability were found to be 0.15 for PEEK permeability, 0.22 for PTFE diffusivity and 0.23 for PTFE solubility coefficient, confirming a reasonable level of experimental consistency despite the limited number of repeats. In particular, PVDF shows virtually no variation in any of the measured parameters, while UHMWPE exhibits a slight decrease in permeability—from 8.6 to 8.2 Barrer—as well as a corresponding reduction in solubility. PTFE displays the most noticeable variation, with permeability increasing by approximately 5% (from 10 to 10.5 Barrer), alongside a moderate rise in diffusivity and a slight decrease in solubility. As for PEEK, both diffusion and solubility coefficients increase in the second cycle, although the overall permeability remains nearly unchanged. These results suggest that no significant changes can be observed in the materials upon exposure to liquid CO_2, indicating a high degree of stability under these operating conditions.

Table 1
Properties of polymers analyzed in this work.

Polymer	ρ [g/cm^3]	Thickness [μm]	Crystallinity (%)	T_g [°C]
PEEK	1.30	75	30.9	152
PVDF	1.77	50	52.4[a]	−35 °C[a]
PTFE	2.20	50	48.5[a]	–
UHMWPE	0.93	50	56.0	< −100[b]

[a] T_g Crystallinity data and Tg are retrieved from ref. [34]. PTFE glass transition temperature was not clearly identified.

[b] T_g has not been measured, but is expected to be well below the temperature range of interest for this study [54].

Table 2
LF/NELF characteristic parameters of the penetrant and polymers considered.

Polymer	p* [MPa]	T* [K]	ρ* [kg/L]	Reference
PVDF	575	660	1.76	[34]
PTFE	370	605	2.24	[34,56]
PEEK	630	845	1.34	This work, pVT data from [56]
UHMWPE	425	649	0.905	[41]
CO_2	575	305	1.51	[24]

When analyzing the experimental data, it is evident that the pressure dependence of CO_2 permeability does not show a uniform behaviour across the investigated materials. In fact, the experimental trends do not always exhibit a clear transition in permeability that could be directly associated with the phase change of CO_2. In the case of PVDF and UHMWPE, permeability isotherms undergo a noticeable inflection as the system transitions from gaseous to liquid-like CO_2 densities. After the phase transition, these materials show a constant permeability value at increasing pressure, similar to the behaviour observed for solubility (Fig. 4S in the Supporting Information) thus describing the reduction of the extent of swelling. This particular trend at high-CO_2 pressure was already observed experimentally by Shamu et al. for PDMS dense membrane [18], and described by Ricci et al. for Matrimid [24] and also by Di Carlo et al. for various amorphous rubbery materials [30], attributing it to an increase of the density of the fluid which leads to a fall of the diffusion coefficient in the polymer matrix when CO_2 reaches the high pressure range.

In contrast, PTFE appears to be an exception as it exhibits a rather stable permeability even after the CO_2 phase transition, suggesting a weaker coupling between CO_2 density and polymer transport properties in this specific material. Interestingly, this behaviour may be linked to a more pronounced variation in solubility which remains constant at higher pressure where the CO_2 remains in the liquid state. Such solubility-driven effects may explain the drastic pressure response observed for PTFE.

As for PEEK, PTFE displays consistently a decreasing permeability with pressure across the entire range of investigated conditions, without any apparent transition-related feature, even though very limited data points are located near or above the transition line. This behaviour suggests that the phase change has limited influence on the transport mechanism in this material. Such effect may also be covered by a dominant role of polymer rigidity and reduced segmental mobility, thus limiting the increase of CO_2 diffusivity, even at elevated pressures and temperatures.

In addition to the pressure dependence, the temperature behaviour of CO_2 permeability offers further insight into the governing transport mechanisms in these semicrystalline thermoplastics.

In general, the permeability is found to decrease with decreasing temperature, suggesting that the kinetic component governs the flow [57]. As temperature rises, the increased segmental mobility of the polymer chains enhances CO_2 diffusivity, whereas solubility, being an exothermic process, typically follows an opposite behaviour (see Fig. 4S in SI). The net effect is an overall increase in permeability with temperature in most of the materials studied. This trend holds for PVDF, UHMWPE, and PEEK, which all show a monotonic increase in permeability with temperature. However, PTFE once again displays a distinctive behaviour: no clear or consistent temperature dependence can be identified across the measured range. This irregularity suggests that, especially at high pressure, sorption phenomena may begin to dominate the transport behaviour, possibly due to the proximity to the CO_2 phase transition and the relatively lower solubility of CO_2 in PTFE at higher temperatures.

To further investigate and rationalize these observations,

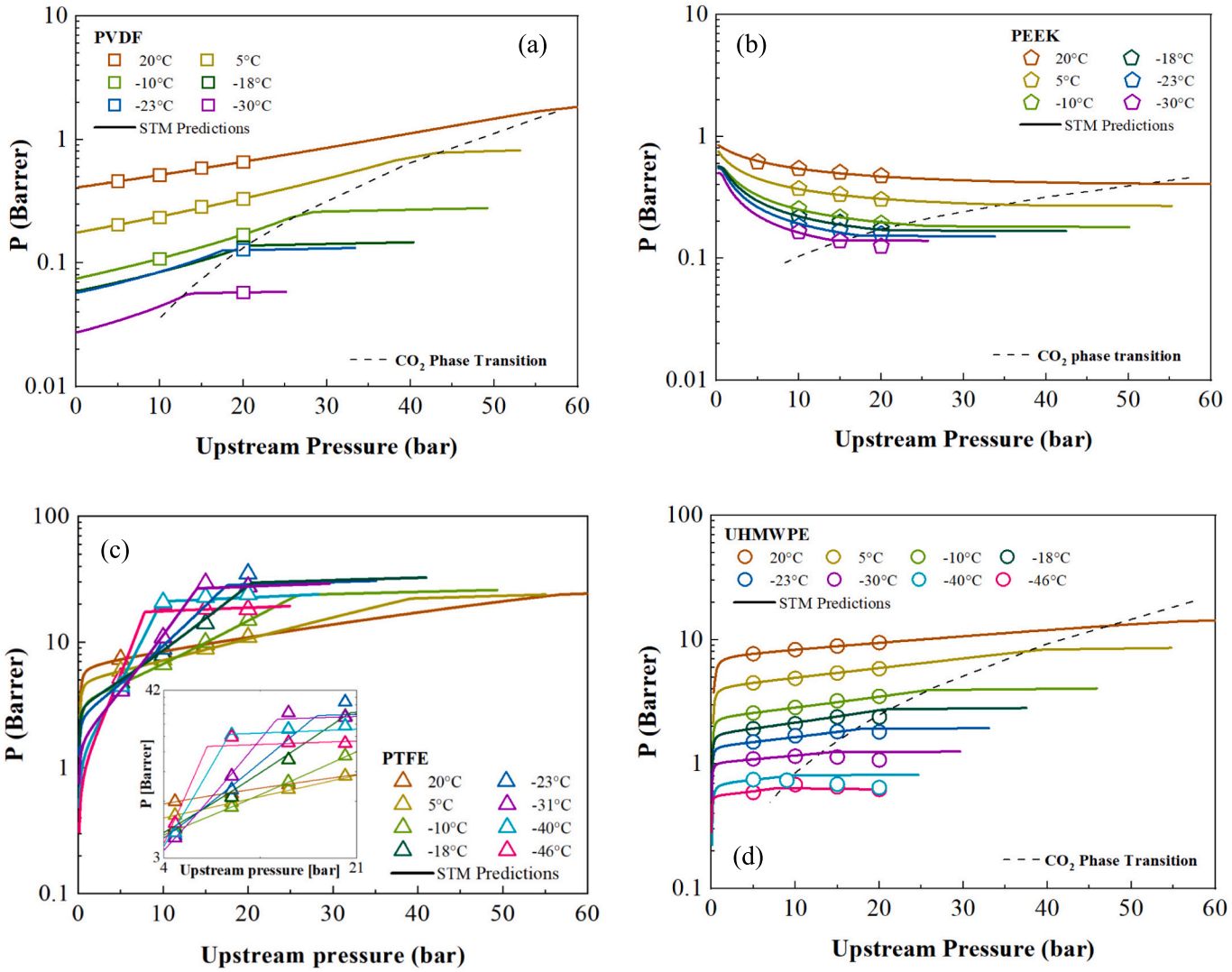

Fig. 2. Experimental permeability data (symbols) coupled with Standard transport model (lines) for semicrystalline polymers: (a) PVDF, (b) PEEK, (c) PTFE, (d) UHMWPE. Different scales have been used for clarity.

particularly the interplay between solubility, diffusion and permeation with temperature and pressure, a more detailed thermodynamic analysis

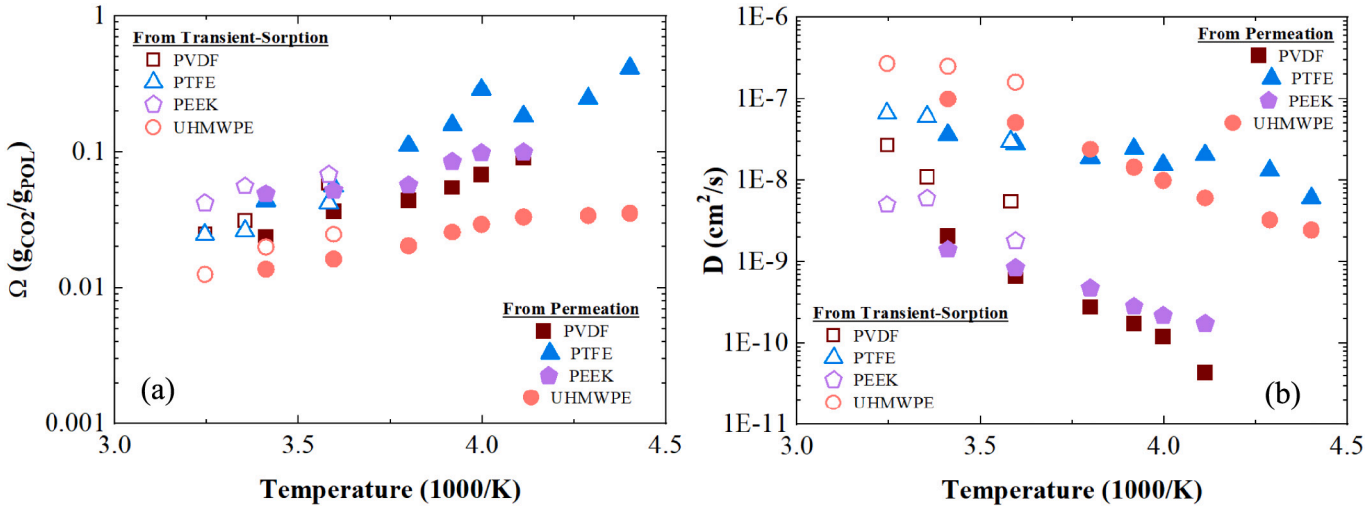

Fig. 3. Data obtained for the different thermoplastic materials at 20 bar (a) Solubility and (b) Diffusivity. Each plot reports a comparison between data obtained from transient-sorption (empty symbols) and those related to permeability (full symbols) for semicrystalline materials.

was carried out. To verify the consistency of the experimental approach and to enable interpretation based on fundamental models and equations of state (EoS), solubility and diffusion coefficients at 20 bar, calculated from transient-sorption experiments and from time lag method (examples of how diffusion coefficients are calculated for both type of experiments are reported in Fig. 7S in the SI) [58], have been compared for the four thermoplastics as a function of temperature (Fig. 3).

The two sets of diffusivity and solubility data show good agreement with each other, supporting the reliability of the results. Although some experimental datasets, such as those for PVDF and UHMWPE, exhibit slight discrepancies, these differences remain within a 30% relative error for solubility and 15% for diffusion coefficients. Moreover, as expected, the solubility increases by decreasing the operating temperature following the Van't Hoff Eq. [59], while diffusion coefficients present an opposite trend with temperature, as predicted by Arrhenius [60].

4.3. CO_2 transport model

In order to better understand the CO_2 transport properties in thermoplastics at low temperatures, a phenomenological model was successfully employed to capture the general behaviour of the permeability using a limited number of adjustable parameters. The Standard Transport Model (STM) approach provides a simple and reliable expression for the determination of gas permeability in glassy and rubbery polymers based on temperature, pressure (or fugacity), and concentration. Such an approach can describe the material performances when exposed to a penetrant by factoring the permeability in a kinetic and thermodynamic contribution by multiplying the rate at which a molecule can diffuse in a polymer matrix with the interactions that the polymer-penetrant mixture molecules may establish [22,23]. The model, which uses the infinite dilution mobility coefficient L_∞ and the plasticization factor β as key outputs of the temperature-dependent analysis, not only fits the data well within at all the different temperature and pressure ranges, but it also allows for an extrapolated interpretation of the transport properties beyond the experimental limits.

First of all, to obtain the most reliable data, the starting point is to determine the solubility isotherms for the same polymer-penetrant gas pair in a wide range of pressure and various temperatures. Fig. 4S in the SI shows the data for CO_2 sorption in the four thermoplastics obtained experimentally from pressure decay technique, coupled with the calculated results from LF/NELF EoS. Continuous lines represent the predictions of the Lattice Fluid model for CO_2 vapour, while the dotted lines correspond to liquid CO_2. The LF EoS reproduces the change in slope of the solubility isotherm associated with the transition between gas-like and liquid-like densities of CO_2. It is noteworthy that the Sanchez Lacombe LF approach, both at equilibrium or non-equilibrium (NELF), effectively describes the thermodynamic behaviour of polymeric and polymer + penetrant systems, but it is less accurate in the representation of CO_2 phase change, often resulting in an overestimation of the vapour pressure. The solubility isotherms exhibit a sharp inflection point at the CO_2 vapour pressure, indicative of the incompressibility of liquid phases. Post-transition, solubility remains relatively constant as the chemical potential of liquid CO_2 exhibits minimal pressure dependence. As a result, the solubility of liquid CO_2 in both thermoplastics and elastomers across varying temperatures closely mirrors the CO_2 sorption behaviour at the respective vapour pressure.

Modelling the CO_2 sorption in PVDF presents additional challenges, as the pure polymer is initially in the rubbery state at ambient temperature due to the sorbed concentration of CO_2 which lowered the glass transition temperature [43,61,62]. Correspondingly, the sorption isotherms shape for polymers in the rubbery state (like PVDF and UHMWPE) present a more convex shape toward x-axes, in contrast with PEEK which is below T_g. A special mention should be made of PTFE which displays distinct relaxation behaviour due to the immobilization of its amorphous phase by the crystalline domains [63]. As observed by Sauer et al. [64], semicrystalline PTFE presents sub-glass transition relaxation (β and γ). Notably, the γ relaxation occurs around 120 °C, while the β relaxation process, that is around −70 °C, is attributed to its glass-to-rubber transition, while as the fully amorphous counterpart of semicrystalline PTFE remains in a rubbery state across the entire temperature range studied in this work, while the crystalline domains broaden the relaxation spectrum [54].

Due to the complex and controversial nature of PTFE's molecular structure and the ambiguity surrounding its glass transition temperatures, this polymer was modelled using the lattice fluid framework at a constant crystallinity. Once the solubility isotherms in the range of interest have been determined by the thermodynamic equation of state (EoS), the results obtained have been coupled with the STM approach to provide a reliable representation of gas transport, according to Eq. (9). Focusing on Fig. 2, where the continuous lines represent the STM-predicted permeability isotherms, these curves are obtained by fitting the model parameters L_∞ and β to the experimental data at different temperatures, as already reported in other works [12,21,24].

The STM approach provides a simple and reliable expression for the determination of gas permeability in glassy and rubbery polymers based on temperature, pressure (and fugacity), and concentration, despite each polymer exhibits a different permeability trend. This allows not only the understanding of the penetrant-polymer interaction and the effect of dense phase CO_2 on polymer-based materials, but it allows the prediction of gas leak (permeation) through the polymer layer in a wide range of temperatures and pressures. Therefore, solubility and permeability isotherms can be calculated according to the following procedure: at each temperature, the adjustable parameter of k_{ij} for the LF and both k_{ij} and k_{swell} for NELF, were optimized on the experimental solubility data as target for the best-fit. The k_{ij} values obtained obey a linear temperature dependence, which are reported in Table 3, so it is quite straightforward to extrapolate these parameters at the desired temperature required by the STM. Similarly, the same procedure is done for permeability from which the best fit to the experimental data allowed the extraction of L_∞ and β as a function of temperature.

To assess the reliability of the model, a sensitivity analysis was performed using the symmetric mean absolute percentage error (sMAPE) which indicates its effectiveness in describing CO_2 transport behaviour. Overall, the average sMAPE for the solubility model is around 5%, with peaks ranging from 10% to 15% for UHMWPE. For permeability, the sMAPE does not exceed 2%, having a maximum around 6% for PTFE prediction at low temperatures. The specific sMAPE values for each isothermal line may be found in Table 2S in the Supplementary Information.

The agreement between the experimental data and the modelling approach is quite good for all the polymer investigated, despite the different behaviours observed (either permeability increases or decreases with temperature and pressure), as visible in Fig. 2.

Moreover, the diffusivity model used in this work incorporates an exponential relationship between CO_2 content and the kinetic component of the diffusion coefficient, commonly known as mobility coefficient (Eq. (9)). The mobility analysis is supported by Fig. 5S in SI, where the diffusion coefficient calculated via Fick's law from sorption data reveals that under infinite dilution conditions (where the

Table 3
Adjustable parameters for the LF, NELF, and ST models used in sorption and transport calculations.

Polymer	CO_2 solubility (LF/NELF)	CO_2 diffusivity (STM)
	k_{ij}	L_∞ (cm^2/s)[a]
PVDF	$1.27\bullet10^{-4}$ T – $5.30\bullet10^{-2}$	1.24 exp. [−5728*/RT]
PTFE	$1.36\bullet10^{-4}$ T - $1.78\bullet10^{-2}$	823 exp. [−6704/RT]
PEEK	$1.06\bullet10^{-3}$ T + $7\bullet10^{-2}$	$3.28\bullet10^{-4}$ exp. [−3561/RT]
UHMWPE	$5.19\bullet10^{-4}$ T + $6.11\bullet10^{-2}$	3.12 exp. [−4753/RT]

[a] Activation energy units: J/mol; R = 8.314 J/mol K.

thermodynamic factor $\alpha \rightarrow 1$), the mobility coefficient L_∞ is similar to D, effectively representing the CO_2 diffusion coefficients measured via pressure-decay experiments. The small differences between L and D observed are attributable to the non-monotonic behaviour of the thermodynamic factor α which is itself the derivative of the sorbed concentration with respect to fugacity (Eq. (10)), associated with CO_2 phase transitions within the polymer. Therefore, the modelling curves are generated by considering a monotonous trend with L_∞ following an Arrhenius dependence on temperature, while similarly, β presented an exponential trend with the inverse of temperature, as visible in Fig. 4 [12,21,24].

As one can see, the PTFE shows the highest plasticization factor among the four, reaching values as high as 90, and a mobility coefficient more than one order of magnitude higher than PVDF and PEEK. Moreover, PTFE is the only one of the materials tested here whose plasticization factor increases by decreasing the temperature, suggesting that the presence of CO_2 at low temperature causes an increase in swelling, thus producing a larger plasticization factor, which also results in an unusual permeability trend with pressure and temperature.

To better highlight both the practical relevance and the fundamental insights of transport phenomena offered by the data, it is scientifically valuable to reorganize the results in a way that facilitates the interpretation of temperature-dependent trends and their implications for potential applications. In the analysis of CO_2 permeability through various polymeric materials, it is generally observed that permeability increases exponentially with temperature. This behaviour, however, does not hold for all polymers. For instance, the PTFE tested here displays an atypical and non-linear trend in CO_2 permeability under low-temperature conditions and medium-high pressure (15/20 bar), deviating significantly from the behaviour observed for the other polymers (Fig. 5).

For dense polymers, permeability is defined as the product of solubility and diffusion coefficients [36] and the interplay between these two parameters, each with its own distinct dependence on temperature and pressure, can lead to complex permeability trends across different materials (Fig. 6S in SI). For PTFE, at low temperatures and high pressures, solubility plays a dominant role. Under these conditions, the increased amount of sorbed CO_2 (due to higher gas density and favourable interactions) results in a rise in permeability. However, as the temperature increases, the solubility coefficient decreases while diffusivity increases, leading to a shift in the dominant mechanism (Fig. 6S). In this regime, the rise in D does not fully compensate for the drop in S, resulting in an overall decrease or plateau in permeability. This behaviour is in line with literature observations reporting significant free volume and chain rigidity effects in PTFE, which influence its gas transport properties [29,65,66]. This is clearly visible when permeability is plotted as a function of temperature at different pressure. Nevertheless, by coupling together the STM approach with the exponential dependence of the mobility coefficient previously obtained, it is possible to describe also the isobaric trend of CO_2 permeability.

Additionally, once the CO_2 content in the polymer has been determined, the thermodynamic EoS model can be employed to evaluate the overall swelling behaviour of the four thermoplastics upon sorption at 20 bar and the same temperature conditions of permeation. Fig. 6 reports the prediction obtained, showing a linear response of the mixture specific volume with the inverse of temperature as long as the CO_2 remains in gaseous state. When CO_2 undergoes the phase transition at 20 bar (~ −20 °C) becoming liquid, the impact is reduced, with swelling showing negligible variations at lower temperatures.

The model provides an interesting prediction of the amorphous phase swelling, as the modelling parameters (k_{ij} and k_{swell}) were optimized independently from temperature and pressure condition for each polymer. Among the investigated materials, PTFE exhibits the largest volume expansion over the entire temperature range, consistent with the strong affinity between CO_2 and fluorinated polymer. This interaction is indicative of significant material swelling, as already observed from gas sorption, which creates additional free volume for penetrant molecules, thus resulting in higher permeability [52,67] and generating the trends observed in Figs. 2 and 5. Conversely, UHMWPE and PEEK show the smallest volume variation under identical CO_2 exposure conditions, indicating a reduced susceptibility to sorption-induced swelling. Finally, PVDF shows an intermediate volumetric expansion compared to the other investigated materials, likely due to the great CO_2 solubility in the amorphous region of the polymer, as already observed in Fig. 4S, but with low permeability values.

5. Conclusion

This work presents a combined experimental and modelling investigation of CO_2 sorption, swelling, and transport in examples of PVDF, PTFE, PEEK, and UHMWPE over a wide range of temperatures and pressures, including sub-ambient and dense-phase CO_2 conditions relevant to transport applications. The lattice fluid–based thermodynamic framework accurately describes CO_2 solubility and the associated volumetric response of the amorphous polymer phase, demonstrating robust predictive capability across the investigated materials and operating conditions.

The integration of sorption and transport data through dedicated modelling provides essential insight into the effects of CO_2 on

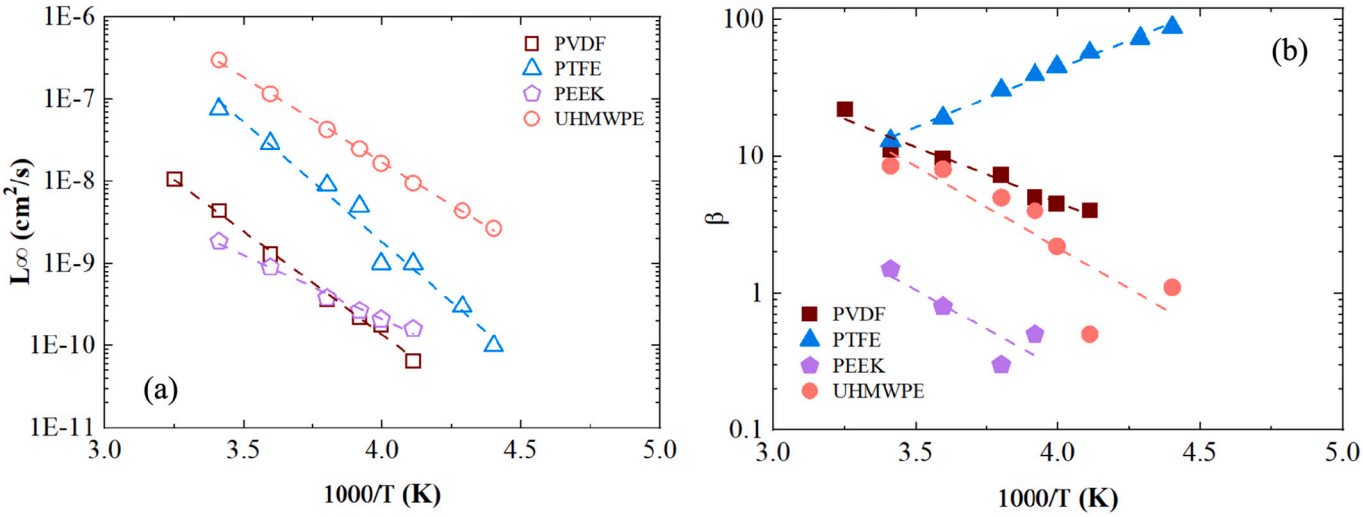

Fig. 4. (a) Infinite dilution mobility coefficient and (b) plasticization factor behaviour as a function of temperature. Dotted lines are used as a guide for the eyes.

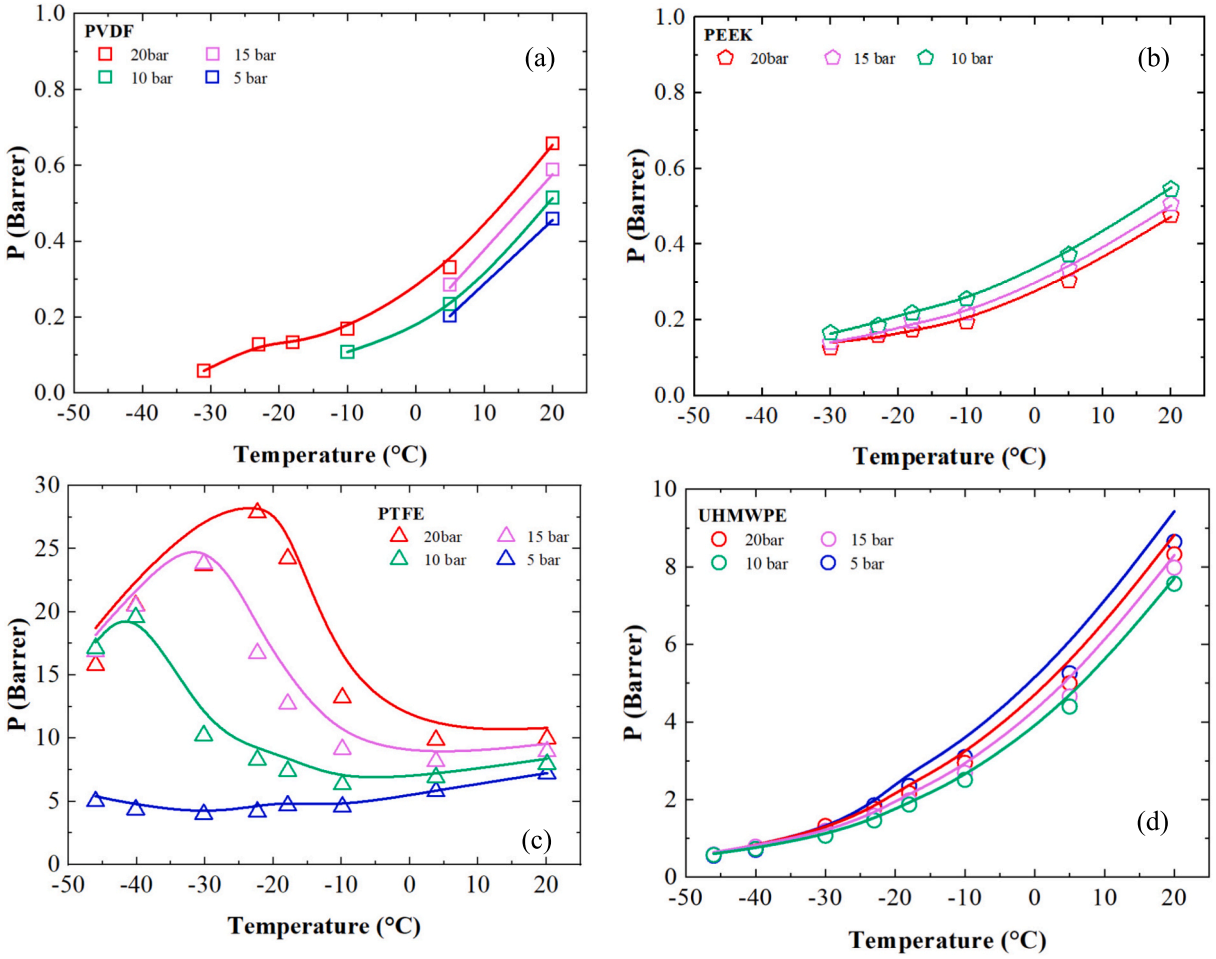

Fig. 5. Isobar trend for (a) PVDF, (b) PEEK, (c) PTFE and (d) UHMWPE as a function of temperature. The isobar lines were calculated using Eq. (9), although for the mobility coefficient L, the trend line obtained through the ST model used for the permeability isotherms was considered. Different scales have been used for clarity .

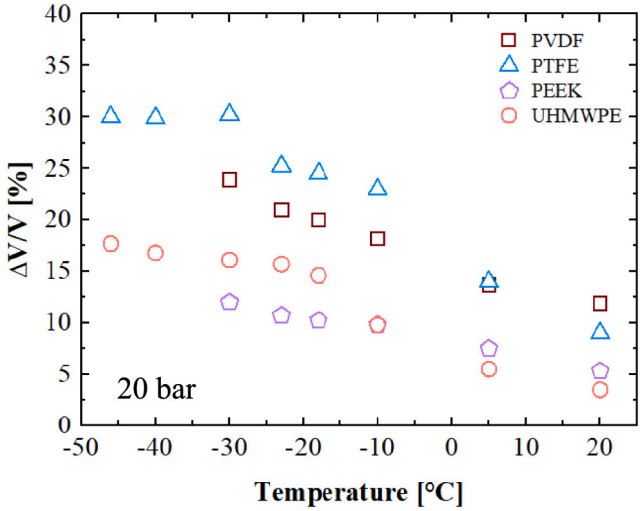

Fig. 6. Average swelling prediction at 20 bar, according to the LF and NELF model, as a function of temperature for the four different polymers.

thermoplastic polymers under conditions representative of CO_2 transportation, spanning from dense to supercritical states. In this context, the Solution–Diffusion Transport Model (STM) successfully reproduces the observed permeability trends and remains fully consistent with the experimental measurements, reinforcing the reliability of the adopted thermodynamic–transport approach for predicting leakage phenomena in liners and sealing elements.

From an application-oriented perspective, low CO_2 solubility is a key factor in limiting gas leakage and minimizing sorption-induced swelling during operation, while an appropriate balance between solubility and diffusivity is required to mitigate the risk of rapid gas decompression damage. Materials exhibiting low solubility combined with sufficiently high diffusivity are expected to retain less CO_2 within the polymer matrix and to release it more efficiently upon sudden changes in the external chemical potential. Among the investigated materials, the PEEK that was tested here combines the lowest permeability with minimal swelling under CO_2 exposure. These characteristics indicate superior resistance to both gas transport and dimensional instability, supporting its selection for critical components within the CO_2 transport chain and contributing to the identification of safer and more reliable polymeric materials for CO_2 infrastructure.

CRediT authorship contribution statement

L. Ansaloni: Writing – review & editing, Methodology, Investigation, Formal analysis, Conceptualization. **V. Signorini:** Writing – original draft, Software, Methodology, Investigation, Formal analysis. **T.A. Peters:** Writing – review & editing, Investigation, Conceptualization. **M. Giacinti Baschetti:** Writing – review & editing, Supervision. **M. Minelli:** Writing – review & editing, Supervision, Methodology, Conceptualization. **B. Alcock:** Writing – review & editing, Project

administration, Methodology, Conceptualization.

Declaration of competing interest

The authors declare that they have no known competing financial interests or personal relationships that could have appeared to influence the work reported in this paper.

Acknowledgments

The authors acknowledge the financial support of the Research Council of Norway and the CLIMIT programme, under grant 308765 (CO_2 EPOC project) and grant 245822 linked to the European Carbon Capture and Storage laboratory Infrastructure (ECCSEL CCS RI, SINTEF MLAB). The research is also supported by the National Recovery and Resilience Plan, Mission 4 Component 2 Investment 3.1 "Fund for the realisation of an integrated system of research and innovation infrastructures"- Call for tender No. 3264 of 28 December 2021 of the Italian Ministry of University and Research funded by the European Union—NextGenerationEU—PNRR IR0000020, Concession Decree No. 244 of 8 August 2022 adopted by the Italian Ministry of University and Research, CUP F53C22000560006, ECCSELLENT—Development of ECCSEL-R.I. Italian facilities: user access, services and long-term sustainability. PEEK samples kindly supplied by Victrex.

Appendix A. Supplementary data

Supplementary data to this article can be found online at https://doi.org/10.1016/j.cej.2026.177624.

Data availability

Data will be made available on request.

References

[1] Eric Paglia, Charles Parker, Chapter 12: The Intergovernmental Panel on Climate Change: Guardian of Climate Science, (n.d.).
[2] M.L. Khandekar, T.S. Murty, P. Chittibabu, The global warming debate: a review of the state of science, Pure Appl. Geophys. 162 (2005) 1557–1586, https://doi.org/10.1007/S00024-005-2683-X/METRICS.
[3] J.P. Banks, T. Boersma, W. Goldthorpe, Challenges Related to Carbon Transportation and Storage–Showstoppers for CCS, The Global CCS Institute, 2017.
[4] J. Gibbins, H. Chalmers, Carbon capture and storage, Energy Policy 36 (2008) 4317–4322, https://doi.org/10.1016/j.enpol.2008.09.058.
[5] J.C.M. Pires, F.G. Martins, M.C.M. Alvim-Ferraz, M. Simões, Recent developments on carbon capture and storage: an overview, Chem. Eng. Res. Des. 89 (2011) 1446–1460, https://doi.org/10.1016/j.cherd.2011.01.028.
[6] A. Raza, R. Gholami, R. Rezaee, V. Rasouli, M. Rabiei, Significant aspects of carbon capture and storage – a review, Petroleum 5 (2019) 335–340, https://doi.org/10.1016/J.PETLM.2018.12.007.
[7] H. Herzog, Carbon dioxide capture and storage, in: The Economics and Politics of Climate Change, 2015, https://doi.org/10.1093/acprof:osobl/9780199573288.003.0013.
[8] L. Ansaloni, B. Alcock, T.A. Peters, Effects of CO_2 on polymeric materials in the CO_2 transport chain: a review, Int. J. Greenh. Gas Con. 94 (2020) 102930, https://doi.org/10.1016/j.ijggc.2019.102930.
[9] K. Johnsen, K. Helle, S. Røneid, H. Holt, DNV recommended practice: design and operation of CO_2 pipelines, Energy Procedia 4 (2011) 3032–3039, https://doi.org/10.1016/j.egypro.2011.02.214.
[10] I.S. Cole, P. Corrigan, S. Sim, N. Birbilis, Corrosion of pipelines used for CO_2 transport in CCS: is it a real problem? Int. J. Greenh. Gas Con. 5 (2011) 749–756, https://doi.org/10.1016/J.IJGGC.2011.05.010.
[11] H. Lund, T. Flåtten, S.T. Munkejord, Depressurization of carbon dioxide in pipelines- models and methods, in: Energy Procedia, Elsevier Ltd, 2011, pp. 2984–2991, https://doi.org/10.1016/j.egypro.2011.02.208.
[12] S.T. Munkejord, M. Hammer, S.W. Løvseth, CO_2 transport: data and models - a review, Appl. Energy 169 (2016) 499–523, https://doi.org/10.1016/j.apenergy.2016.01.100.
[13] S. Roussanaly, A.L. Brunsvold, E.S. Hognes, Benchmarking of CO_2 transport technologies: part II – offshore pipeline and shipping to an offshore site, Int. J. Greenh. Gas Con. 28 (2014) 283–299, https://doi.org/10.1016/J.IJGGC.2014.06.019.
[14] V. Neela, N. Von Solms, Permeability, diffusivity and solubility of carbon dioxide in fluoropolymers: an experimental and modeling study, J. Polym. Res. 21 (2014), https://doi.org/10.1007/s10965-014-0401-z.
[15] O.M. Davies, J.C. Arnold, S. Sulley, The mechanical properties of elastomers in high-pressure CO_2, J. Mater. Sci. 34 (1998) 417–422.
[16] M.L. Goñi, N.A. Gañán, R.E. Martini, Supercritical CO_2-assisted dyeing and functionalization of polymeric materials: a review of recent advances (2015–2020), J. CO_2 Util. 54 (2021), https://doi.org/10.1016/j.jcou.2021.101760.
[17] W.H. Tuminello, G.T. Dee, M.A. McHugh, Dissolving perfluoropolymers in supercritical carbon dioxide, Macromolecules 28 (1995) 1506–1510, https://doi.org/10.1021/ma00109a023.
[18] A. Shamu, M. Dunnewold, H. Miedema, Z. Borneman, K. Nijmeijer, Permeation of supercritical CO_2 through dense polymeric membranes, J. Supercrit. Fluids 144 (2019) 63–70, https://doi.org/10.1016/j.supflu.2018.10.009.
[19] S. Doroudiani, C.B. Park, M.T. Kortschot, Effect of the crystallinity and morphology on the microcellular foam structure of semicrystalline polymers, Polym. Eng. Sci. 36 (1996) 2645–2662, https://doi.org/10.1002/pen.10664.
[20] B.M.M. Bonavoglia, G. Stori, M. Morbidelli, A. Rajendran, Sorption and swelling of Semicrystalline polymers in supercritical CO_2, J. Polym. Sci. B Polym. Phys. 44 (2006) 1531–1546, https://doi.org/10.1002/polb.
[21] M. Minelli, M.G. De Angelis, An equation of state (EoS) based model for the fluid solubility in semicrystalline polymers, Fluid Phase Equilib. 367 (2014) 173–181, https://doi.org/10.1016/j.fluid.2014.01.024.
[22] M. Minelli, G.C. Sarti, Permeability and diffusivity of CO_2 in glassy polymers with and without plasticization, J. Membr. Sci. 435 (2013) 176–185, https://doi.org/10.1016/j.memsci.2013.02.013.
[23] M. Minelli, G.C. Sarti, Permeability and solubility of carbon dioxide in different glassy polymer systems with and without plasticization, J. Membr. Sci. 444 (2013) 429–439, https://doi.org/10.1016/j.memsci.2013.04.007.
[24] E. Ricci, M.G. De Angelis, M. Minelli, A comprehensive theoretical framework for the sub and supercritical sorption and transport of CO_2 in polymers, Chem. Eng. J. 435 (2022) 135013, https://doi.org/10.1016/j.cej.2022.135013.
[25] B. Bonavoglia, G. Storti, M. Morbidelli, Modeling of the sorption and swelling behavior of semicrystalline polymers in supercritical CO_2, Ind. Eng. Chem. Res. 45 (2006) 1183–1200, https://doi.org/10.1021/ie050842c.
[26] I.C. Sanchez, R.H. Lacombe, Statistical thermodynamics of polymer solutions, Macromolecules 11 (1978) 1145–1156, https://doi.org/10.1021/ma60066a017.
[27] F. Doghieri, G.C. Sarti, Nonequilibrium lattice fluids: a predictive model for the solubility in glassy polymers, Macromolecules 29 (1996) 7885–7896, https://doi.org/10.1021/ma951366c.
[28] M. Minelli, G.C. Sarti, Gas permeability in glassy polymers: a thermodynamic approach, Fluid Phase Equilib. 424 (2016) 44–51, https://doi.org/10.1016/J.FLUID.2015.09.027.
[29] S. Matteucci, Y. Yampolskii, B.D. Freeman, I. Pinnau, Transport of gases and vapors in glassy and rubbery polymers, in: Y. Yampolskii, I. Pinnau, B.D. Freeman (Eds.), Materials Science of Membranes for Gas and Vapor Separation, John Wiley & Sons, Ltd, 2006, pp. 1–47, 2006.
[30] R. Di Carlo, E. Ricci, M. Minelli, Comprehensive modelling strategy for gas transport in polymers: analysis of swelling and non-swelling agents at high pressures, Fluid Phase Equilib. 591 (2025) 114311, https://doi.org/10.1016/J.FLUID.2024.114311.
[31] E.R. Larson, Thermoplastic material selection: a practical guide, in: Thermoplastic Material Selection: A Practical Guide, 2015, pp. 1–348, https://doi.org/10.1016/C2013-0-18851-4.
[32] D.M. D'Alessandro, B. Smit, J.R. Long, Carbon dioxide capture: prospects for new materials, Angew. Chem. Int. Ed. (2010), https://doi.org/10.1002/anie.201000431.
[33] S.T. McCoy, E.S. Rubin, An engineering-economic model of pipeline transport of CO_2 with application to carbon capture and storage, Int. J. Greenh. Gas Con. 2 (2008) 219–229, https://doi.org/10.1016/S1750-5836(07)00119-3.
[34] V. Signorini, L. Ansaloni, T. Peters, B. Alcock, M.G. Baschetti, M. Minelli, Characterization and modeling of CO_2 transport through fluorinated thermoplastics, ACS Appl. Polym. Mater. (2023), https://doi.org/10.1021/ACSAPM.3C02056.
[35] D.Y. Peng, D.B. Robinson, A new two-constant equation of state, Ind. Eng. Chem. Fundam. 15 (1976) 59–64, https://doi.org/10.1021/i160057a011.
[36] J.G. Wijmans, R.W. Baker, The solution-diffusion model: a review, J. Membr. Sci. 107 (1995) 1–21, https://doi.org/10.1016/0376-7388(95)00102-I.
[37] E. Ricci, F.M. Benedetti, A. Noto, T.C. Merkel, J. Jin, M.G. De Angelis, Enabling experimental characterization and prediction of ternary mixed-gas sorption in polymers: $C_2H_6/CO_2/CH_4$ in PIM-1, Chem. Eng. J. 426 (2021) 130715, https://doi.org/10.1016/J.CEJ.2021.130715.
[38] J. Crank, The Mathematics of Diffusion 2nd Ed, 79, Claredon Press - Oxford University Press, 1975, pp. 1267–1268, https://doi.org/10.1021/ja01562a072, 1957.
[39] P.J. Flory, Statistical thermodynamics of liquid mixtures, J. Am. Chem. Soc. 87 (1965) 1833–1838, https://doi.org/10.1021/ja01087a002.
[40] P.J. Flory, Thermodynamics of polymer solutions, Discuss. Daraday Society 49 (1970) 683–748, https://doi.org/10.1201/9781420040944.
[41] O. Atiq, E. Ricci, M.G. Baschetti, M.G. De Angelis, Modelling solubility in semi-crystalline polymers: a critical comparative review, Fluid Phase Equilib. 556 (2022) 113412, https://doi.org/10.1016/j.fluid.2022.113412.
[42] M. Minelli, B.R. Pimentel, M.L. Jue, R.P. Lively, G.C. Sarti, Analysis and utilization of cryogenic sorption isotherms for high free volume glassy polymers, Polymer 170 (2019) 157–167, https://doi.org/10.1016/j.polymer.2019.03.012.

[43] R.F. Boyer, Glassy transitions in semicrystalline polymers, J. Polym. Sci. Polym. Symp. 50 (1975) 189–242, https://doi.org/10.1002/POLC.5070500114.
[44] F. Doghieri, M. Quinzi, D.G. Rethwisch, G.C. Sarti, Predicting gas solubility in membranes through non-equilibrium thermodynamics for glassy polymers, Materials Science of Membranes for Gas and Vapor Separation (2006) 137–158, https://doi.org/10.1002/047002903X.CH4.
[45] M.G. Baschetti, F. Doghieri, G.C. Sarti, Solubility in glassy polymers: correlations through the nonequilibrium lattice fluid model, Ind. Eng. Chem. Res. 40 (2001) 3027–3037, https://doi.org/10.1021/IE000834Q.
[46] M. Minelli, G.C. Sarti, 110th anniversary: gas and vapor sorption in glassy polymeric membranes - critical review of different physical and mathematical models, Ind. Eng. Chem. Res. 59 (2020) 341–365, https://doi.org/10.1021/acs.iecr.9b05453.
[47] M. Minelli, G.C. Sarti, Permeability and solubility of carbon dioxide in different glassy polymer systems with and without plasticization, J. Membr. Sci. 444 (2013) 429–439, https://doi.org/10.1016/J.MEMSCI.2013.04.007.
[48] M. Minelli, D.R. Paul, G.C. Sarti, On the interpretation of cryogenic sorption isotherms in glassy polymers, J. Membr. Sci. 540 (2017) 229–242, https://doi.org/10.1016/J.MEMSCI.2017.06.053.
[49] M. Minelli, S. Campagnoli, M.G. De Angelis, F. Doghieri, G.C. Sarti, Predictive model for the solubility of fluid mixtures in glassy polymers, Macromolecules 44 (2011) 4852–4862, https://doi.org/10.1021/MA200602D.
[50] R.H. Lacombe, I.C. Sanchez, Statistical thermodynamics of fluid mixtures, J. Phys. Chem. 80 (1976) 2568–2580, https://doi.org/10.1021/j100564a009.
[51] M. Minelli, F. Doghieri, A predictive model for vapor solubility and volume dilation in glassy polymers, Ind. Eng. Chem. Res. 51 (2012) 16505–16516, https://doi.org/10.1021/ie3021076.
[52] W.J. Jordan, S.S. Koros, A free volume distribution model for gas sorption and dilation in glassy polymers, Macromolecules 28 (1995) 2228–2235.
[53] E. Toni, M. Minelli, G.C. Sarti, A predictive model for the permeability of gas mixtures in glassy polymers, Fluid Phase Equilib. 455 (2018) 54–62, https://doi.org/10.1016/j.fluid.2017.09.025.
[54] Y. Araki, Thermal expansion coefficient of polytetrafluoroethylene in the vicinity of its glass transition at about 400°K, J. Appl. Polym. Sci. 9 (1965) 421–427, https://doi.org/10.1002/app.1965.070090203.
[55] D.W. Green, M.Z. Southard, Perry's Chemical Engineers' Handbook, McGraw-Hill Education, 2019.
[56] W.D. Zoller P., Standard Pressure Volume Temperature Data for Polymers, 1995.
[57] L.M. Costello, W.J. Koros, Temperature dependence of gas sorption and transport properties in polymers: measurement and applications, Ind. Eng. Chem. Res. 31 (1992) 2708–2714, https://doi.org/10.1021/ie00012a012.
[58] H.L. Frisch, The time lag in diffusion, J. Phys. Chem. 61 (1) (1957) 93–95, https://doi.org/10.1021/j150547a018.
[59] J.H. van't Hoff XLVII, The origin of the theory of solutions, Lond. Edinb. Dublin Philos. Mag. J. Sci. 37 (1894) 475–491, https://doi.org/10.1080/14786449408620576.
[60] M. Menzinger, R. Wolfgang, The meaning and use of the Arrhenius activation energy, Angew. Chem. Int. Ed. Eng. 8 (1969) 438–444, https://doi.org/10.1002/ANIE.196904381.
[61] M.C. Shen, A. Eisenberg, Glass transitions in polymers, Rubber Chem. Technol. 43 (1970) 95–155, https://doi.org/10.5254/1.3547245.
[62] T.S. Chow, Glass transition temperature of polymer-diluent systems, Ferroelectrics 30 (1980) 139–145, https://doi.org/10.1080/00150198008209505.
[63] R.H. Boyd, Strengths of the mechanical-, ß-, and 7-relaxation processes in linear polyethylenet analysis of the anelastic relaxation behavior of LPE we begin with, Macromolecules 17 (1984) 903–911.
[64] Peter Avakian, Howard W. Starkweather, J.R. Bryan, B. Sauer, Cooperative relaxations in semicrystalline fluoropolymers studied by thermally stimulated currents and ac dielectric, J. Polym. Sci. B Polym. Phys. 34 (1996) 517–526.
[65] R.A. Pasternak, M.V. Christensen, J. Heller, Diffusion and permeation of oxygen, nitrogen, carbon dioxide, and nitrogen dioxide through polytetrafluoroethylene, Macromolecules 3 (1970) 366–371, https://doi.org/10.1021/ma60015a020.
[66] B.D. Freeman, Basis of permeability/selectivity tradeoff relations in polymeric gas separation membranes, Macromolecules 32 (1999) 375–380, https://doi.org/10.1021/ma9814548.
[67] J.S. Vrentas, J.L. Duda, H.C. Ling, Free-volume equations for polymer-penetrant diffusion, J. Membr. Sci. (1989), https://doi.org/10.1016/S0376-7388(00)80915-1.